APPENDIX N°1

TO THE FINAL TECHNICAL REPORT

CONTRACT N° N68171-97-C-9003

(Final Technical Report 1998)

NUMERICAL STUDY OF STRESS CONCENTRATORS IN IMPACT SHEARING

by

M. Klósak and J.R. Klepaczko

Contractor:
Laboratoire de Physique et Mécanique des Matériaux
UMR CNRS 7554
Institut Supérieur de Génie Mécanique et Productique
UNIVERSITE DE METZ
F-57045 Metz, France

APPENDIX N°1

TO THE FINAL TECHNICAL REPORT

CONTRACT N° N68171-97-C-9003

(Final Technical Report 1998)

NUMERICAL STUDY OF STRESS CONCENTRATORS IN IMPACT SHEARING

by

M. Klósak and J.R. Klepaczko

Contractor:
Laboratoire de Physique et Mécanique des Matériaux
UMR CNRS 7554
Institut Supérieur de Génie Mécanique et Productique
UNIVERSITE DE METZ
F-57045 Metz, France

ABSTRACT

This Appendix contains complete results of numerical calculations by FE code ABAQUS/Explicit for four geometries of a shear layer with different stress concentrators. Those four geometries are shown in Fig. 1 of this Appendix.

All calculations have been performed for VAR 4340 steel with hardness ~50 HRC. Several shear velocities have been assumed, from 10 m/s to 150 m/s.

Because of thermal coupling the local heating around a stress concentrator leads to failure due to carrying capacity of the material. Two local failure criteria have been introduced into the numerical scheme. The first one is based on the maximum inelastic deformation in the adiabatic conditions, and the second one on the concept of the strain energy density, also in the adiabatic case. Both criteria give similar results concerning the failure patterns. A general conclusion can be reached that during impact shearing the failure is more sensitive to the adiabatic stress concentrators at higher impact velocities. The final results are given in the form of graphs and tables.

1. Geometry

Four different specimen geometries were studied and they are presented in Fig. 1. The loading conditions are similar as in the experiments and they are described in the Final Technical Report. It should be only noted that there exists the symmetry in the numerical problem, so only half specimen is considered. The proposed FE models are demonstrated in Fig. 2 a, b, c and d. The general purpose finite element code ABAQUS/Explicit was chosen for the simulations.

2. Boundary conditions

All boundary conditions are shown in Fig. 2. Part A is loaded with a constant velocity and part B is supported. Attachment of a specimen to the Hopkinson tube is provided by the screws that do not assure a complete fixation, but rather serve to place the specimen properly. Such support was modeled by applying contact surfaces between the specimen and the tube. This type of boundary conditions permitted to reflect real phenomena observed at the interface tube-specimen like small local plastification of the specimen, slight rotation of the external parts during impact or separation between the specimen and the tube. The tube was modeled as an infinite elastic half-space.

Impact velocity V(t) was applied at the upper nodes in the specific way, from zero to the maximum value V_m. The total rise-time t_m was chosen according to the Gaussian cumulative distribution function depending on the impact velocity V_i. The mathematical form of the rise-time function is represented by

$$F(x) = \int_{x_{min}}^{x} \frac{1}{\sqrt{2\pi\sigma^2}} \exp\left(-\frac{(X-m)^2}{2\sigma^2}\right) dX$$

Schematic representation of the rise-time function is shown in Fig.3. The constant rise-time was assumed as $t_m = 2 \cdot 10^{-7}$ s. Values of parameters m and σ in are m=0.5, σ=0.125.

3. Constitutive relation

A constitutive relation was sought to reflect plastic behavior of VAR 4340 steel, ~50 HRC, at high strain rates and at wide range of temperature. The explicit form of the constitutive relation is assumed as follows

$$\tau = \frac{\mu(T)}{\mu_o}\left[B\left(\frac{T}{T_o}\right)^{-\nu}\left(\Gamma_o + \Gamma\right)^n + \tau_o\left(1 - \frac{T}{D}\log\frac{\dot{\Gamma}_o}{\dot{\Gamma}}\right)^m\right]$$

where B, μ_O, υ, n, m are respectively, the modulus of plasticity, the shear modulus at T=300 K, the temperature index, the strain hardening exponent and the logarithmic rate sensitivity, T_O, Γ_O and $\dot{\Gamma}_O$ are normalisation constants, and $\mu(T)$ is given by

$$\mu(T) = \mu_o[1-A(\Delta T)-C(\Delta T)^2]; \quad \Delta T = T - T_R$$

where τ and Γ are respectively the shear stress and shear strain, A, C are constants.
It should be noted that application of the constitutive equation is restricted to $T \geq 300$ K.

The strain hardening exponent n is a linearly decreasing function of temperature

$$n(T) = n_o(1-T/T_m)$$

where n_o is the strain hardening exponent at T=0 K and T_m is the melting temperature.
All constants for VAR 4340 steel are presented in Table 1.

Table 1. Material constants for VAR4340 steel, ~50 HRC

Const.	Value	Unit	Const.	Value	Unit
B	1493.0	MPa	A	$5.047 \cdot 10^{-4}$	1/K
μ_O	80769.0	MPa	C	$1.036 \cdot 10^{-7}$	$1/K^2$
υ	0.39	-	D	2914.0	K
n	n(T) in text	-	τ_O	622.0	MPa
n_o	0.135	-	β	0.9	-
m	2.776	-	λ	38.0	W/mK
T_o	300.0	K	ρ	7890.0	kg/m^3
Γ_o	$1.6 \cdot 10^{-3}$	-	C_v	460.0	J/kgK
$\dot{\Gamma}_o$	10^6	1/s	T_m	1812.0	K

A failure criterion based on the critical inelastic deformation Γ_{pc} was introduced in the constitutive relation. Specific value of Γ_{pc} was obtained from the instability point $\partial\tau/\partial\Gamma=0$ on the adiabatic τ-Γ curves. A failure criterion based on the critical energy density, where the critical plastic work dissipated during deformation was found by integration of the adiabatic τ-Γ curve up to the instability point $\partial\tau/\partial\Gamma=0$, was also introduced. Both approaches give similar results and they are compared in Fig. 4.

The FE simulations were carried out with the thermal coupling. Since a large part of the plastic work is converted into heat, the deformed material heats up. The balance of energy with the heat conduction leads to the following relation

$$\beta\tau\frac{\partial\Gamma}{\partial t}=\rho C_v\frac{\partial T}{\partial t}-\lambda\frac{\partial^2 T}{\partial y^2}$$

where y is the axis of the heat conduction and λ is the heat conductivity (Fourier constant). Material constants associated with the process of thermal coupling are also given in Table 1.

The approach to the thermal coupling which is formulated above permits for numerical analyses of all temperature-coupled problems as purely adiabatic as well as with the heat conduction. When the process is entirely adiabatic, $\lambda = 0$ (no heat conduction), the heating is uniform in an elementary volume. Because of a short time scale, this assumption was applied to all FE simulations.

4. Simulation data

Several impact velocities were considered, from 10 m/s to 150 m/s. Standard geometry was of the main interest, additional impact velocities were added for this type of geometry in order to observe the Critical Impact Velocity in shear which was estimated as ~130 m/s.
All simulation impact velocities are given in Table 2.

Table 2. Simulation velocities

Impact velocity	Geometry of the specimen			
V_i [m/s]	Standard	U-geometry	V-geometry	Sharp notch
10	X	X	X	X
30	X	X	X	X
60	X	X	X	X
80	X	X	X	X
100	X	X	X	
115	X			
130	X	X	X	
150	X			

5. Tables and graphs with obtained results

The values presented in Table 3 were found from the graphs presented hereafter to give a quick comparison of the values obtained. The detailed analysis and discussion of the results is given in the Final Technical Report.

Table 3. Results from the numerical simulations

Geometry	V impact [m/s]	R max [kN]	δ 1 [mm]	Γ 1	δ 2 [mm]	Γ 2	Energy [J]
Q	10	49,4	0,138	0,069	0,312	0,156	7,11
	30	61,2	0,181	0,091	0,362	0,181	6,68
	60	62,4	0,053	0,027	0,465	0,233	7,51
	80	54,6	0,037	0,019	0,322	0,161	5,05
	100	55	0,033	0,017	0,239	0,120	4,25
	115	53,1	0,035	0,018	0,241	0,121	4,07
	130	48,3	0,039	0,020	0,228	0,114	2,62
	150	28,7	0,025	0,013	0,195	0,098	2,59
U	10	45,4	0,231	0,116	0,345	0,173	9,22
	30	58,7	0,235	0,118	0,372	0,186	9,18
	60	66,4	0,304	0,152	0,381	0,191	10,69
	80	67,1	0,184	0,092	0,417	0,209	11,03
	100	63,5	0,119	0,060	0,366	0,183	8,61
	130	52,3	0,064	0,032	0,331	0,166	6,11
V	10	47,9	0,087	0,044	0,182	0,091	3,52
	30	59,3	0,111	0,056	0,197	0,099	3,92
	60	52,6	0,061	0,031	0,229	0,115	5,04
	80	46,4	0,046	0,023	0,247	0,124	5,43
	100	44,9	0,043	0,022	0,228	0,114	5,4
	130	55,7	0,059	0,030	0,241	0,121	5,29
N	10	49,4	0,053	0,027	0,079	0,040	1,37
	30	55,4	0,061	0,031	0,095	0,048	1,58
	60	38,4	0,021	0,011	0,098	0,049	1,49
	80	36,5	0,011	0,006	0,091	0,046	1,37

Rmax maximum reaction force,

δ1 displacement of the central part of the DS geometry at the beginning of failure (elimination of the first element),

Γ1 corresponding nominal shear strain (=δ1/hs, hs=2.0 mm),

δ2 displacement of the central part of the DS geometry at the final failure (the last element eliminated).

Γ2 corresponding nominal shear strain (=δ1/hs, hs=2.0 mm),

Energy dissipated plastic energy.

FIGURE CAPTIONS

Fig. 1 Specimen geometries with different stress concentrators.

Fig. 2 FE mesh for four models; a/ standard geometry, b/ U-geometry, c/ V-geometry, d/ geometry with a sharp notch.

Fig. 3 Graphical representation of the Gaussian Cumulative Function.

Fig. 4 Criteria of failure applied in FE calculations.

Fig. 5 Crack propagation in standard specimen; V_i = 10 m/s.

Fig. 6 Crack propagation in U specimen; V_i = 10 m/s.

Fig. 7 Crack propagation in V specimen; V_i = 10 m/s.

Fig. 8 Crack propagation in specimen with sharp notch; V_i = 10 m/s.

Fig. 9 Temperature distribution at shear layer at failure, V_i = 10 m/s, a/ standard geometry, b/ U geometry, c/ V geometry, d/ sharp notch geometry.

Fig. 10 Plastic equivalent strain distribution at failure, V_i = 10 m/s; a/ standard geometry, b/ U geometry, c/ V geometry, d/ sharp notch geometry.

Fig. 11 Displacement of the central part of the DS geometry at the beginning of failure (elimination of the first element).

Fig. 12 Displacement of the central part of the DS geometry at the final failure (the last element eliminated).

Fig. 13 Dissipated plastic energy vs. impact velocity; 4 types of specimen geometry.

Fig. 14 Reaction force vs. time for the chosen impact velocities; 4 types of specimen geometry; a/ V_i = 10 m/s, b/ V_i = 80 m/s, c/ V_i = 130 m/s.

Fig. 15 Maximum reaction force as a function of impact velocity; 4 types of specimen geometry; a/ linear scale, b/ logarithmic scale.

Fig. 16 Nominal shear stress vs. nominal shear strain curves for the standard geometry.

Fig. 17 Nominal shear stress vs. nominal shear strain curves for the U-geometry.

Fig. 18 Nominal shear stress vs. nominal shear strain curves for the V-geometry.

Fig. 19 Nominal shear stress vs. nominal shear strain curves for the sharp notch geometry.

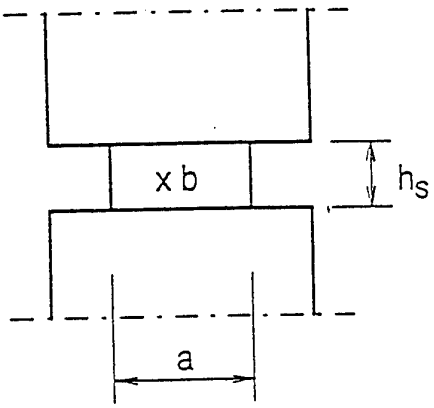

(a)

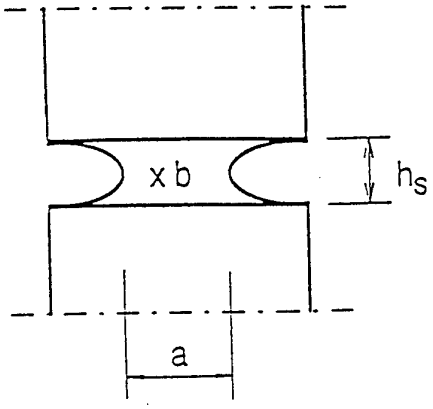

(b)

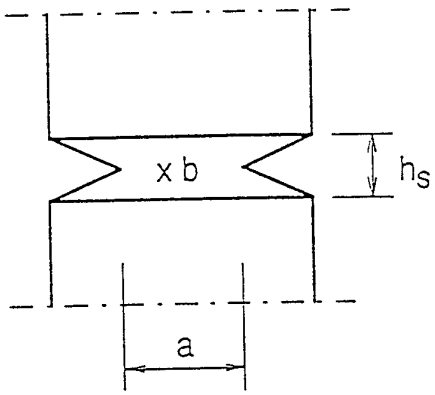

(c)

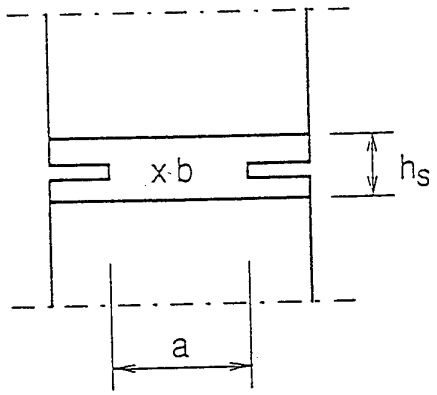

(d)

Fig. 1

ABAQUS

Standard geometry

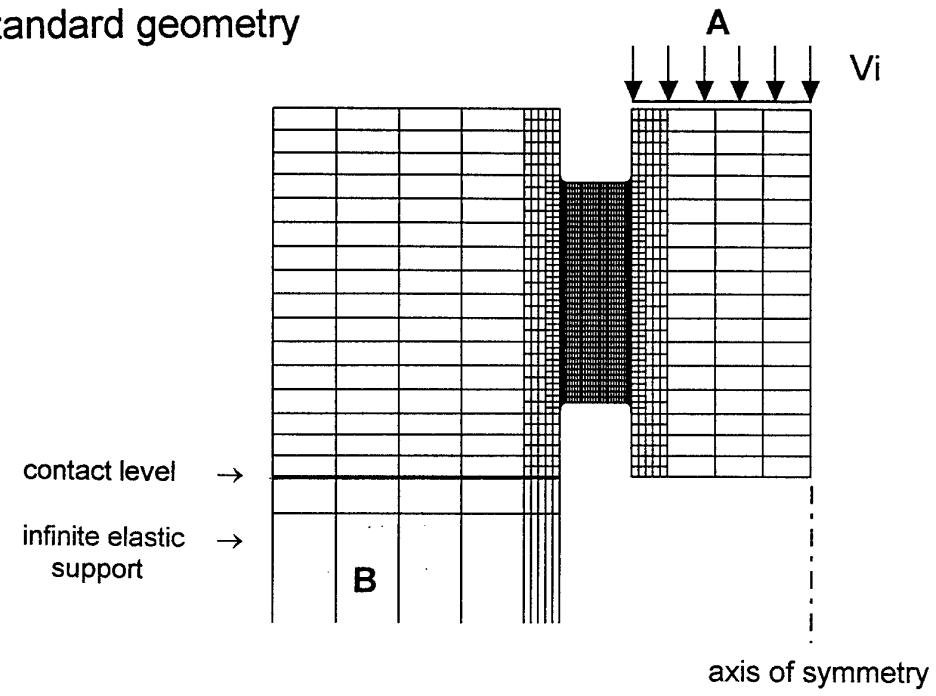

a/

ABAQUS

U-geometry

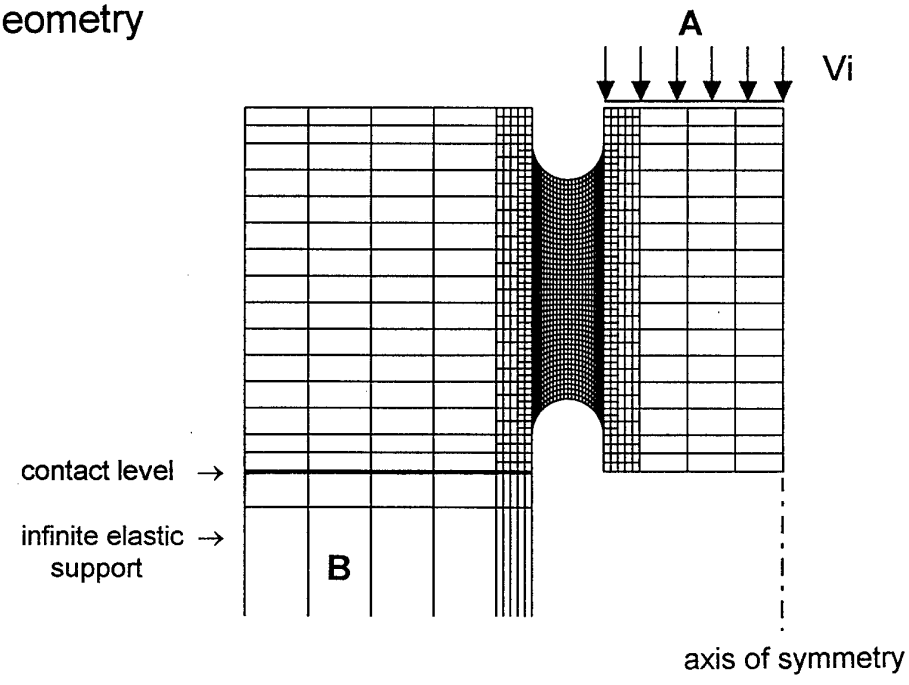

b/

Fig. 2

ABAQUS

V-geometry

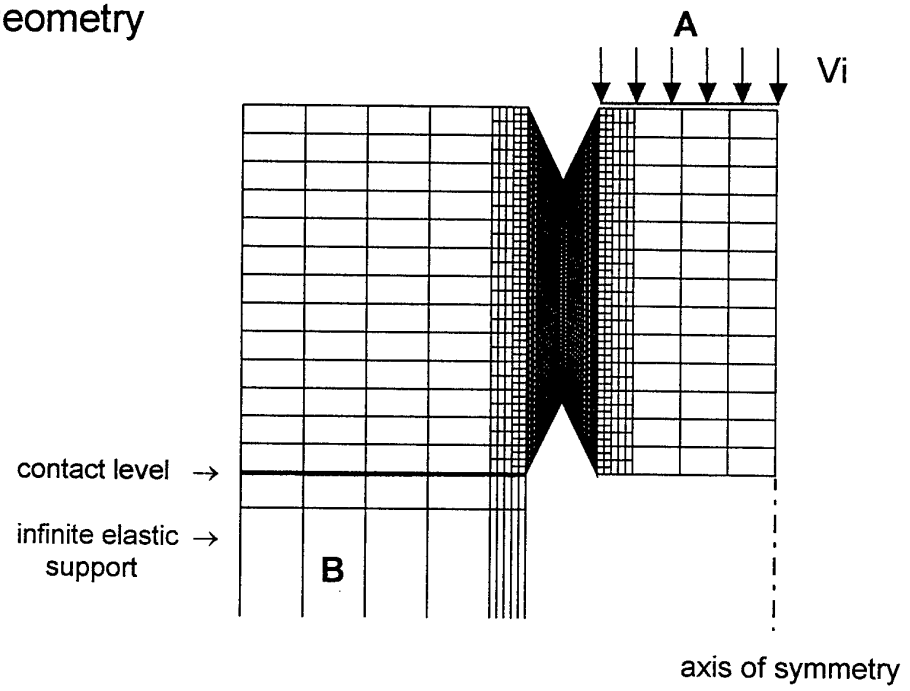

c/

ABAQUS

Sharp notch geometry

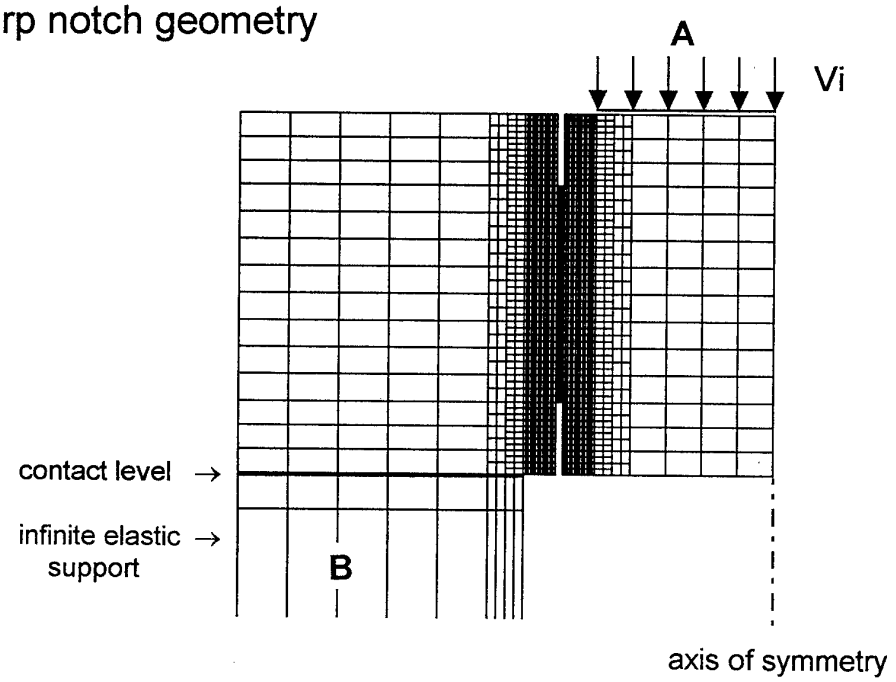

d/

Fig. 2

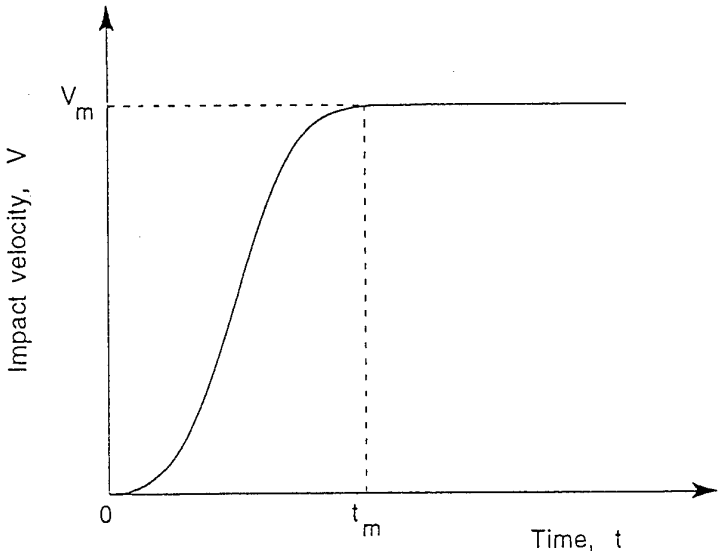
Impact velocity, V
V_m
0
t_m
Time, t

Fig. 3

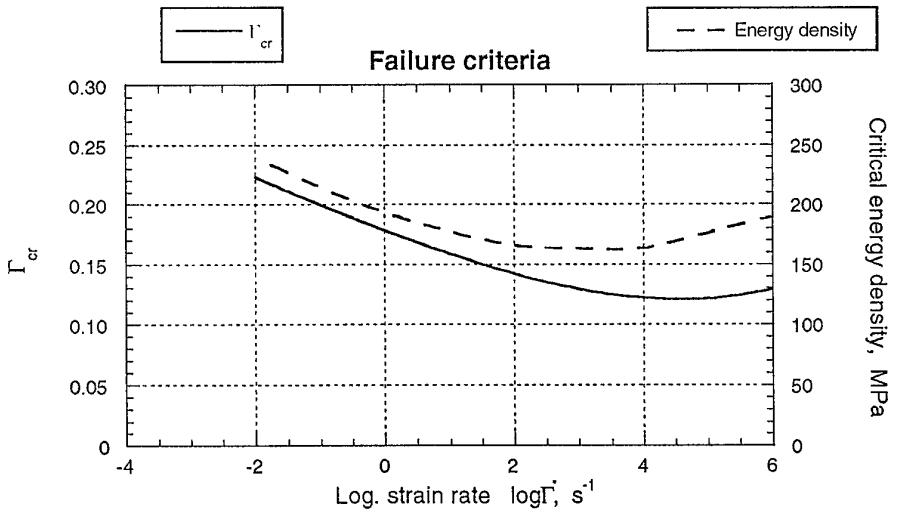
Γ_{cr}
Energy density
Failure criteria
0.30
0.25
0.20
0.15
0.10
0.05
0
Γ_{cr}
300
250
200
150
100
50
0
Critical energy density, MPa
-4
-2
0
2
4
6
Log. strain rate $\log\dot{\Gamma}$, s^{-1}

Fig. 4

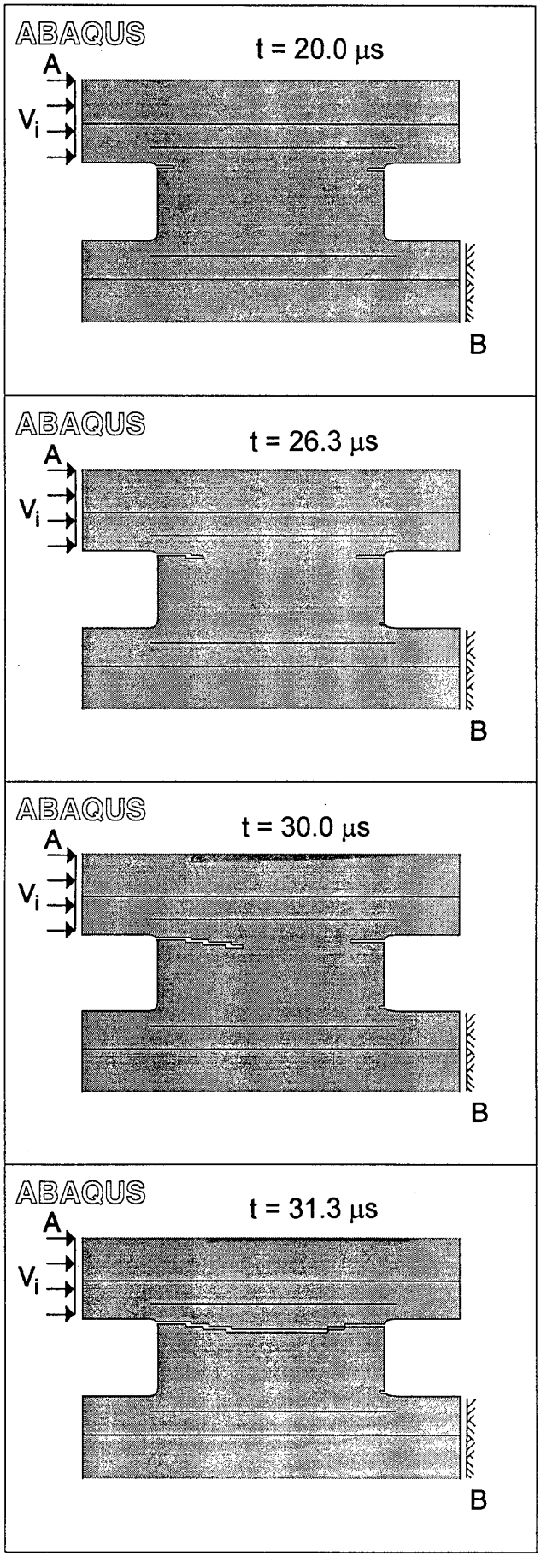
ABAQUS
t = 20.0 μs
A
V_i
B
ABAQUS
t = 26.3 μs
A
V_i
B
ABAQUS
t = 30.0 μs
A
V_i
B
ABAQUS
t = 31.3 μs
A
V_i
B

Fig. 5

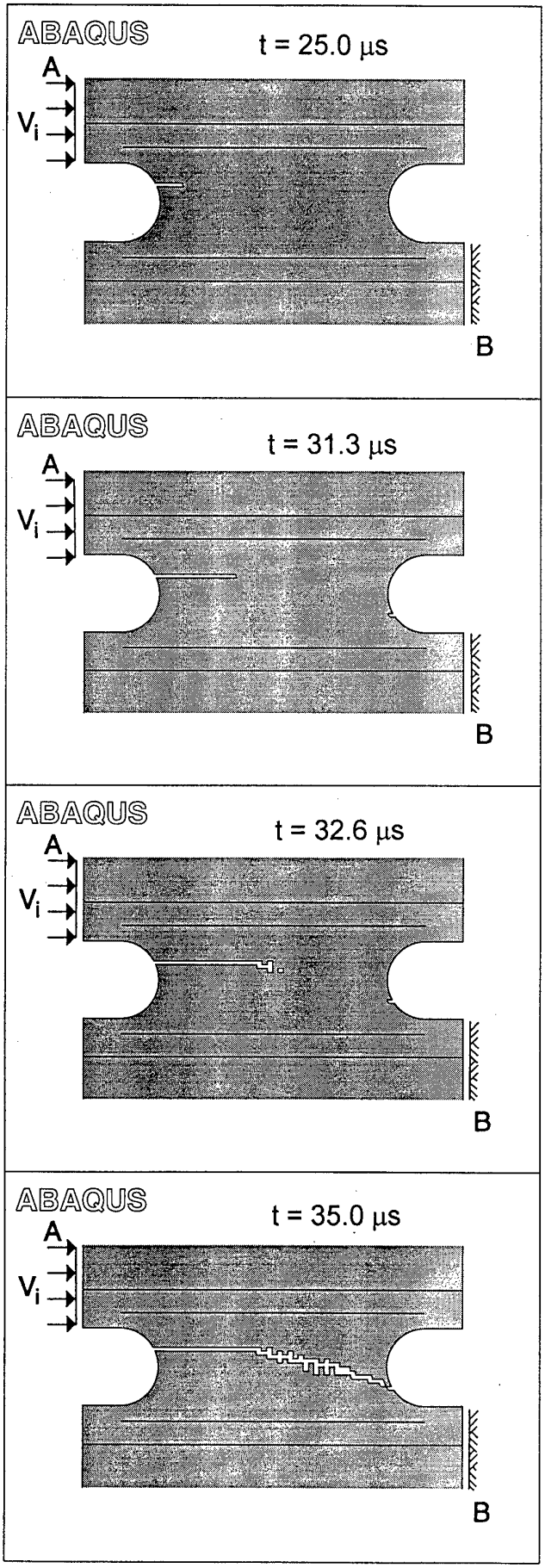
ABAQUS
t = 25.0 μs
A
V_i
B
ABAQUS
t = 31.3 μs
A
V_i
B
ABAQUS
t = 32.6 μs
A
V_i
B
ABAQUS
t = 35.0 μs
A
V_i
B

Fig. 6

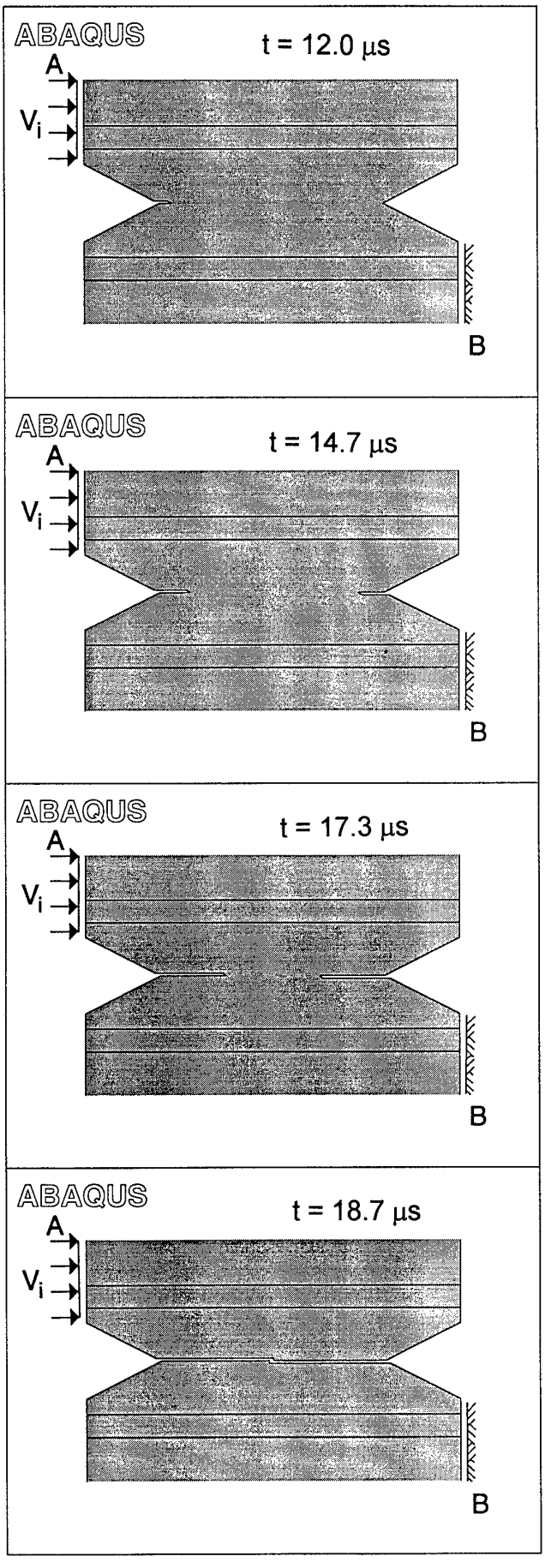
ABAQUS
t = 12.0 μs
A
V_i
B
ABAQUS
t = 14.7 μs
A
V_i
B
ABAQUS
t = 17.3 μs
A
V_i
B
ABAQUS
t = 18.7 μs
A
V_i
B

Fig. 7

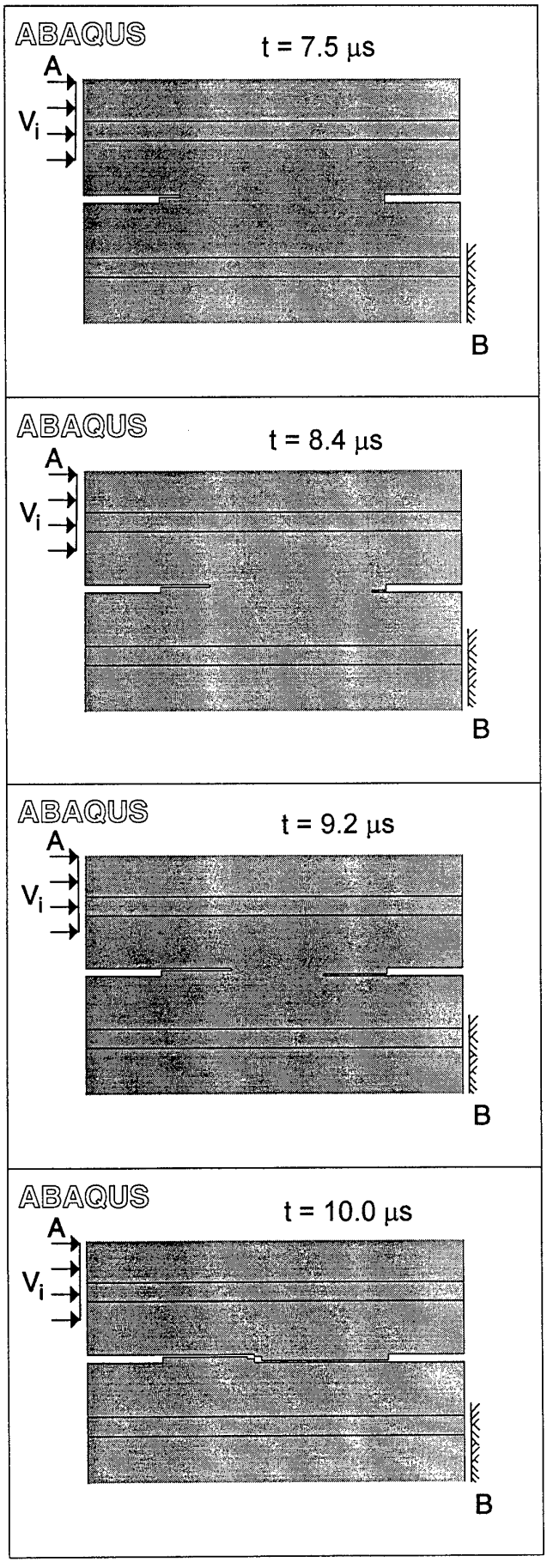
ABAQUS
t = 7.5 μs
A
Vi
B
ABAQUS
t = 8.4 μs
A
Vi
B
ABAQUS
t = 9.2 μs
A
Vi
B
ABAQUS
t = 10.0 μs
A
Vi
B

Fig. 8

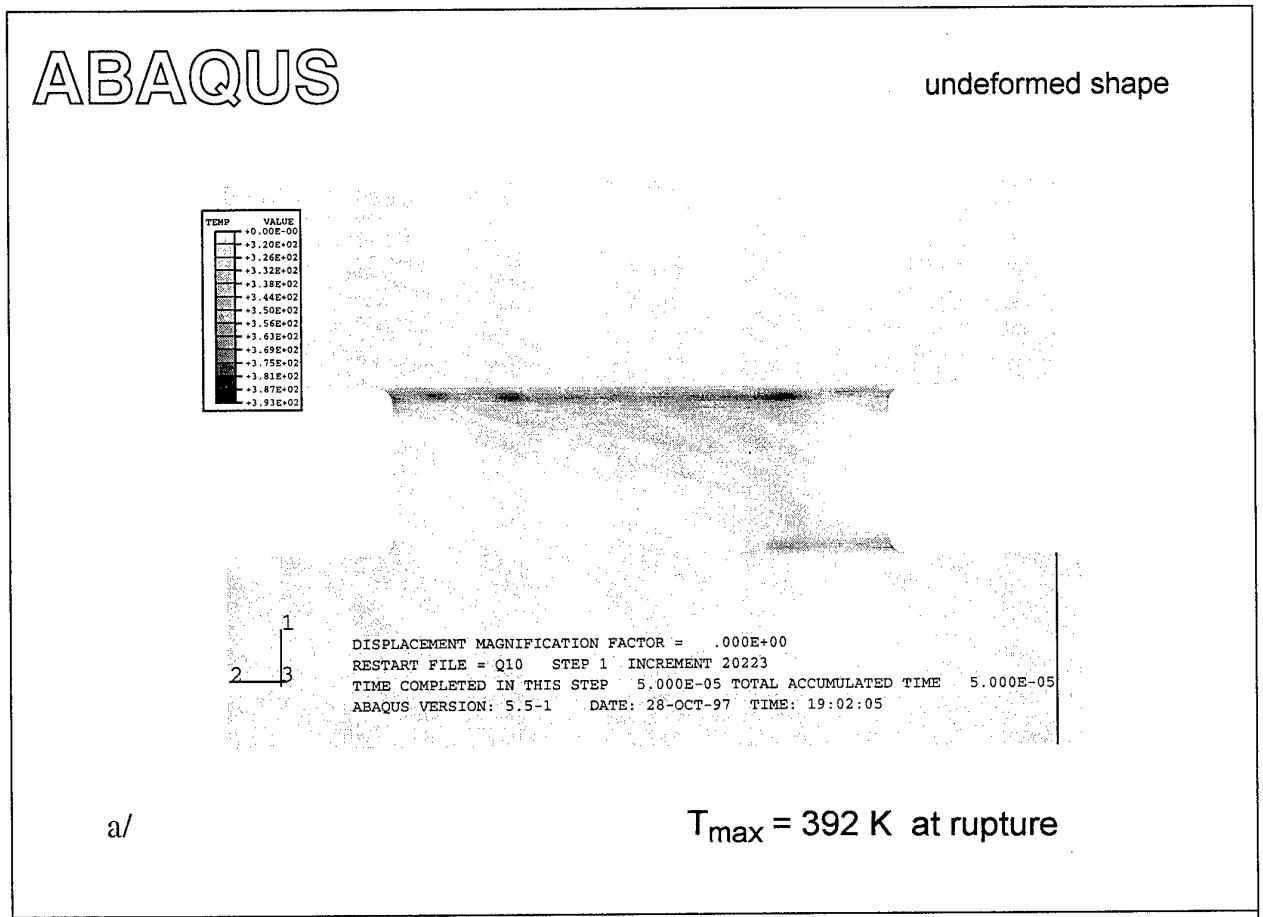
ABAQUS
undeformed shape
TEMP
VALUE
+0.00E-00
+3.20E+02
+3.26E+02
+3.32E+02
+3.38E+02
+3.44E+02
+3.50E+02
+3.56E+02
+3.63E+02
+3.69E+02
+3.75E+02
+3.81E+02
+3.87E+02
+3.93E+02
1
2
3
DISPLACEMENT MAGNIFICATION FACTOR = .000E+00
RESTART FILE = Q10 STEP 1 INCREMENT 20223
TIME COMPLETED IN THIS STEP 5.000E-05 TOTAL ACCUMULATED TIME 5.000E-05
ABAQUS VERSION: 5.5-1 DATE: 28-OCT-97 TIME: 19:02:05
a/
T_{max} = 392 K at rupture

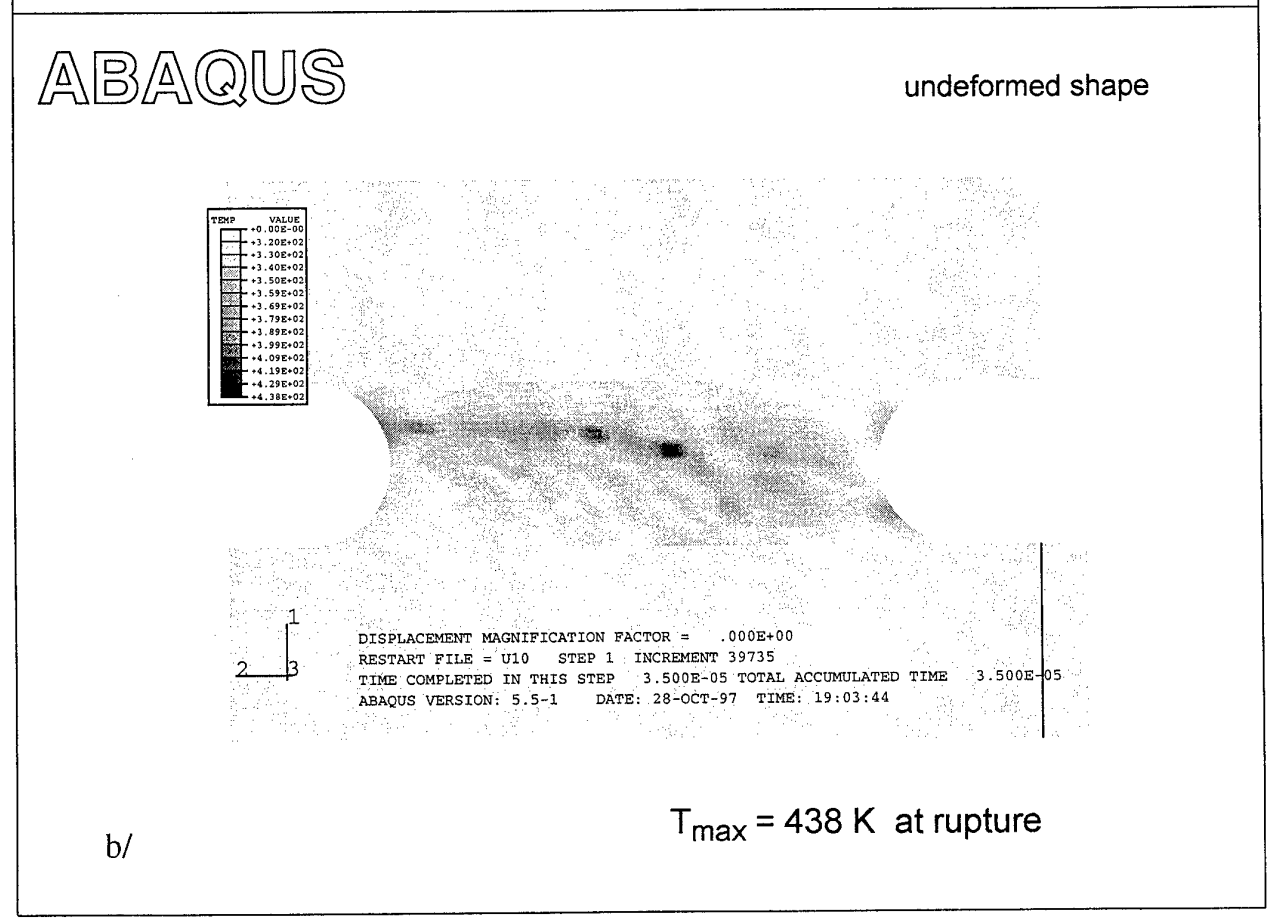
ABAQUS
undeformed shape
TEMP
VALUE
+0.00E-00
+3.20E+02
+3.30E+02
+3.40E+02
+3.50E+02
+3.59E+02
+3.69E+02
+3.79E+02
+3.89E+02
+3.99E+02
+4.09E+02
+4.19E+02
+4.29E+02
+4.38E+02
1
2
3
DISPLACEMENT MAGNIFICATION FACTOR = .000E+00
RESTART FILE = U10 STEP 1 INCREMENT 39735
TIME COMPLETED IN THIS STEP 3.500E-05 TOTAL ACCUMULATED TIME 3.500E-05
ABAQUS VERSION: 5.5-1 DATE: 28-OCT-97 TIME: 19:03:44
b/
T_{max} = 438 K at rupture

Fig. 9

ABAQUS

undeformed shape

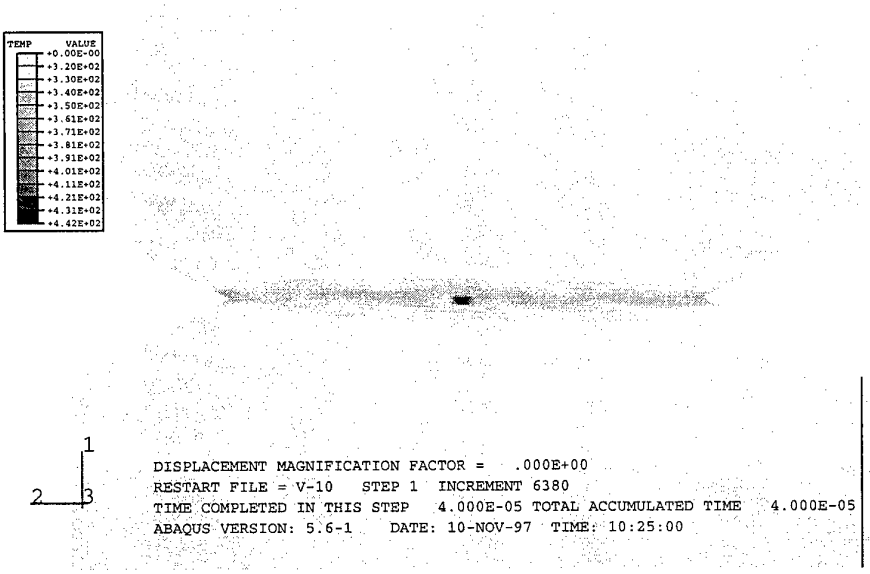

c/

T_{max} = 441 K at rupture

ABAQUS

undeformed shape

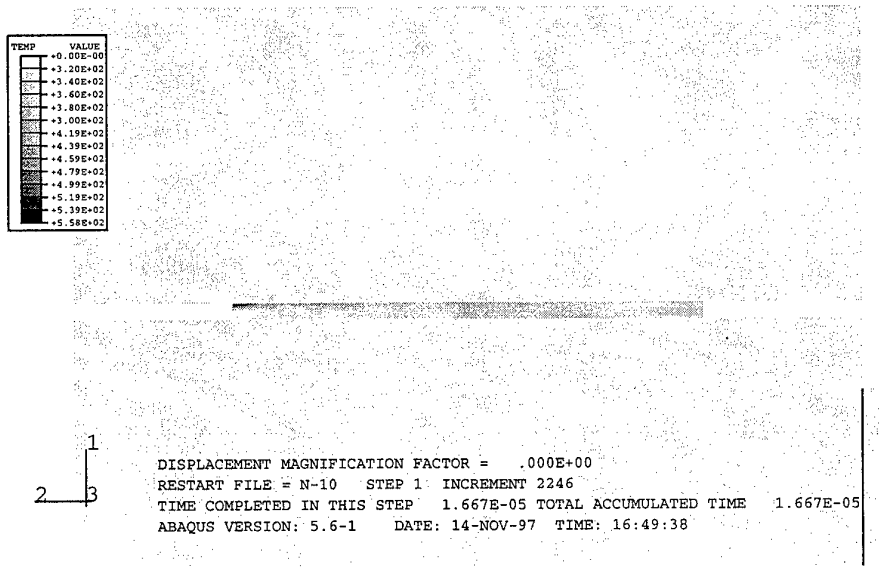

d/

T_{max} = 558 K at rupture

Fig. 9

ABAQUS

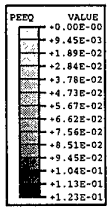

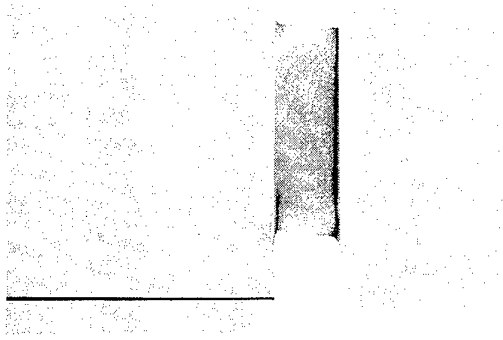

DISPLACEMENT MAGNIFICATION FACTOR = 1.00
RESTART FILE = Q10 STEP 1 INCREMENT 12657
TIME COMPLETED IN THIS STEP 3.125E-05 TOTAL ACCUMULATED TIME 3.125E-05
ABAQUS VERSION: 5.5-1 DATE: 28-OCT-97 TIME: 19:02:05

$t_{rupture} = 31.3\ \mu s \quad \Gamma_{n\ rupture} = 0.156$

a/

ABAQUS

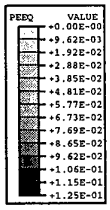

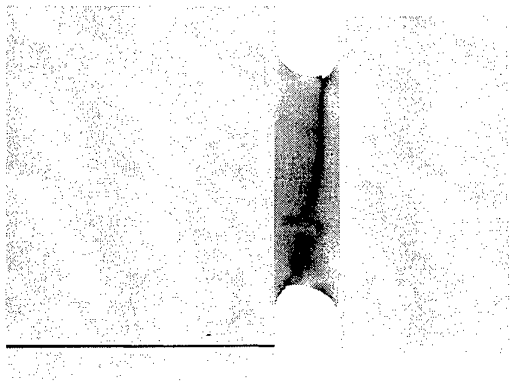

DISPLACEMENT MAGNIFICATION FACTOR = 1.00
RESTART FILE = U10 STEP 1 INCREMENT 39735
TIME COMPLETED IN THIS STEP 3.500E-05 TOTAL ACCUMULATED TIME 3.500E-05
ABAQUS VERSION: 5.5-1 DATE: 28-OCT-97 TIME: 19:03:44

$t_{rupture} = 35.0\ \mu s \quad \Gamma_{n\ rupture} = 0.173$

b/

Fig. 10

ABAQUS

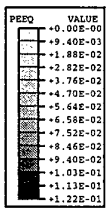

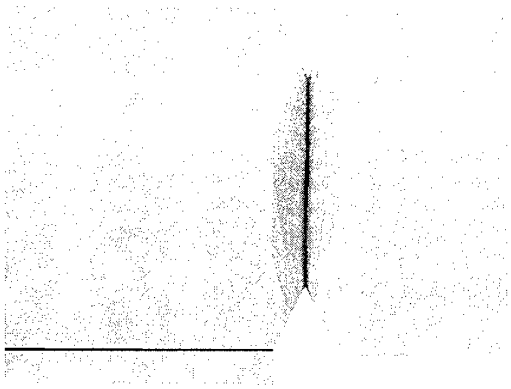

DISPLACEMENT MAGNIFICATION FACTOR = 1.00
RESTART FILE = V-10 STEP 1 INCREMENT 3013
TIME COMPLETED IN THIS STEP 1.867E-05 TOTAL ACCUMULATED TIME 1.867E-05
ABAQUS VERSION: 5.6-1 DATE: 10-NOV-97 TIME: 10:25:00

c/ $t_{rupture} = 18.7\ \mu s \quad \Gamma_{n\ rupture} = 0.091$

ABAQUS

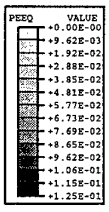

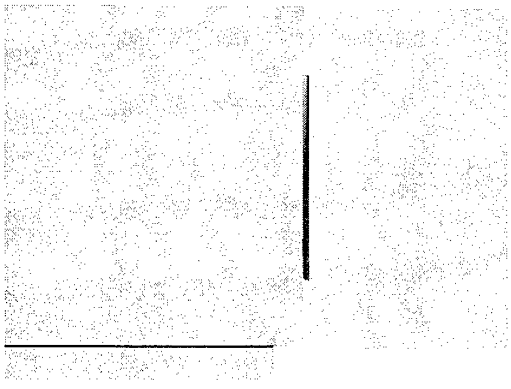

DISPLACEMENT MAGNIFICATION FACTOR = 1.00
RESTART FILE = N-10 STEP 1 INCREMENT 1328
TIME COMPLETED IN THIS STEP 1.001E-05 TOTAL ACCUMULATED TIME 1.001E-05
ABAQUS VERSION: 5.6-1 DATE: 14-NOV-97 TIME: 16:49:38

d/ $t_{rupture} = 10.0\ \mu s \quad \Gamma_{n\ rupture} = 0.040$

Fig. 10

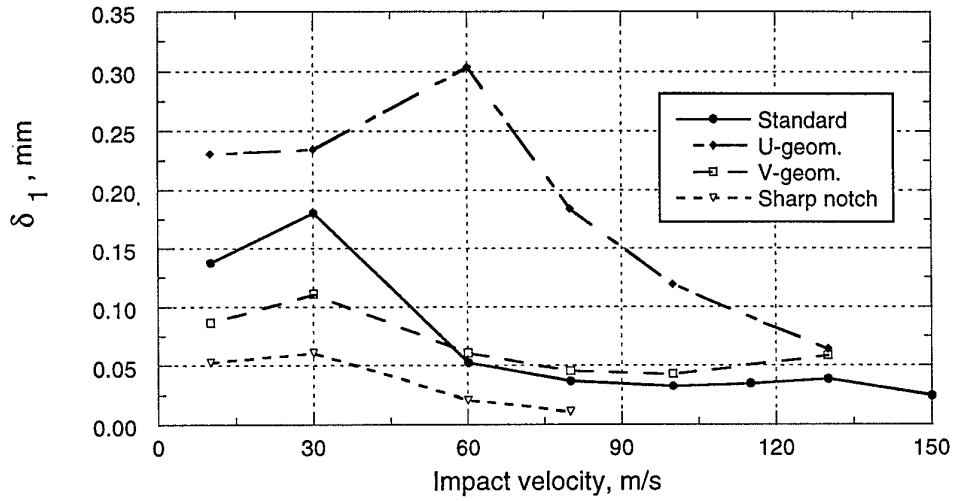
0.35
0.30
0.25
0.20
0.15
0.10
0.05
0.00
δ 1 , mm
0
30
60
90
120
150
Impact velocity, m/s
Standard
U-geom.
V-geom.
Sharp notch

Fig. 11

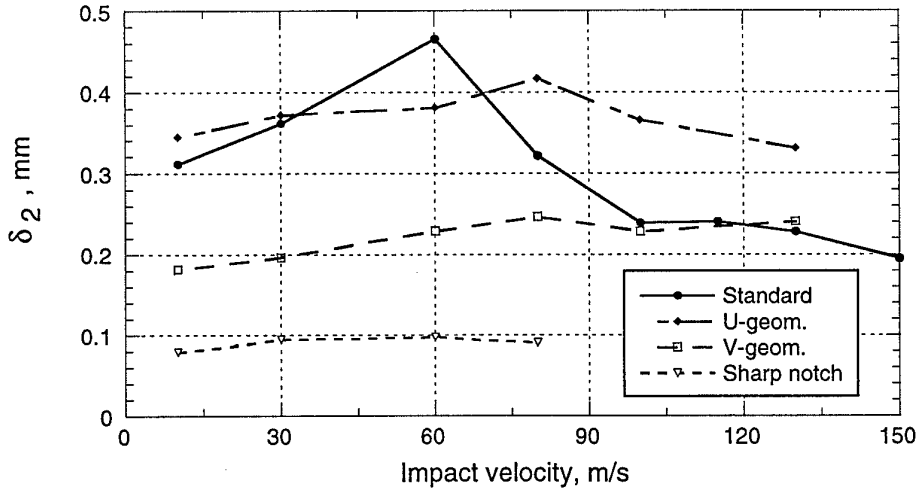
0.5
0.4
0.3
0.2
0.1
0
δ 2 , mm
0
30
60
90
120
150
Impact velocity, m/s
Standard
U-geom.
V-geom.
Sharp notch

Fig. 12

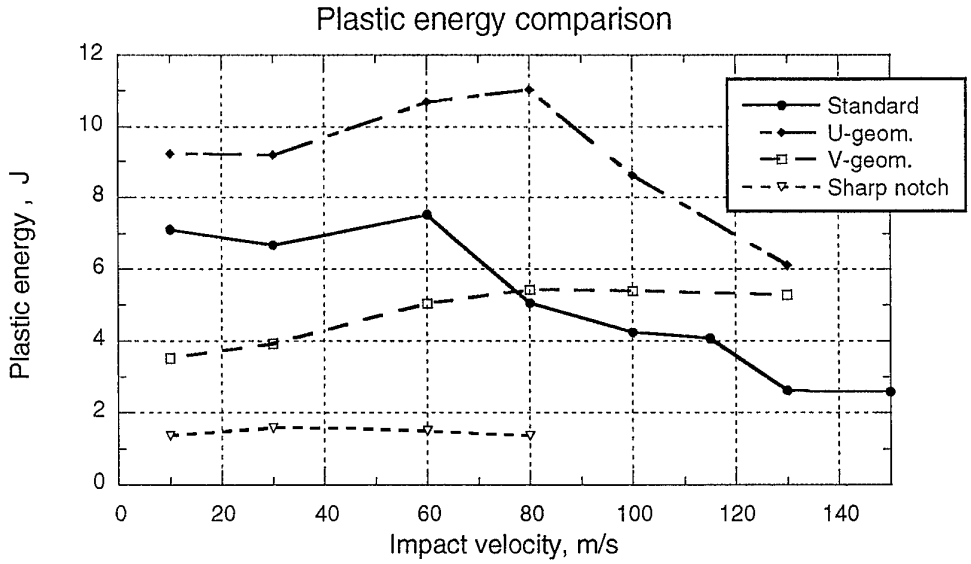
Plastic energy comparison
Plastic energy , J
Impact velocity, m/s
0
2
4
6
8
10
12
0
20
40
60
80
100
120
140
Standard
U-geom.
V-geom.
Sharp notch

Fig. 13

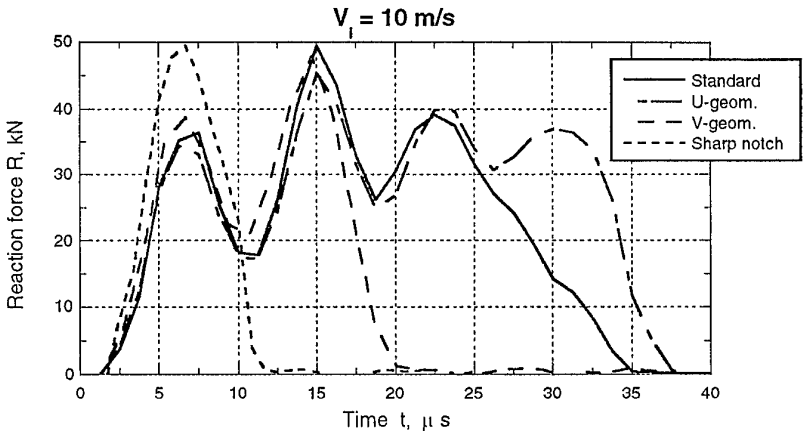
V_i = 10 m/s
Reaction force R, kN
Time t, μ s
Standard
U-geom.
V-geom.
Sharp notch

a/

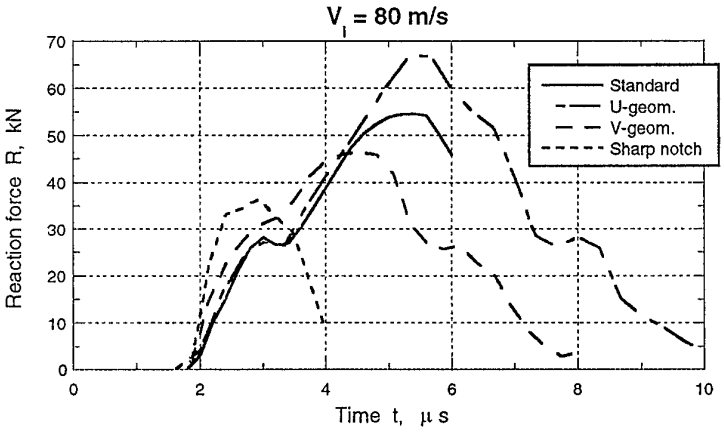
V_i = 80 m/s
Reaction force R, kN
Time t, μ s
Standard
U-geom.
V-geom.
Sharp notch

b/

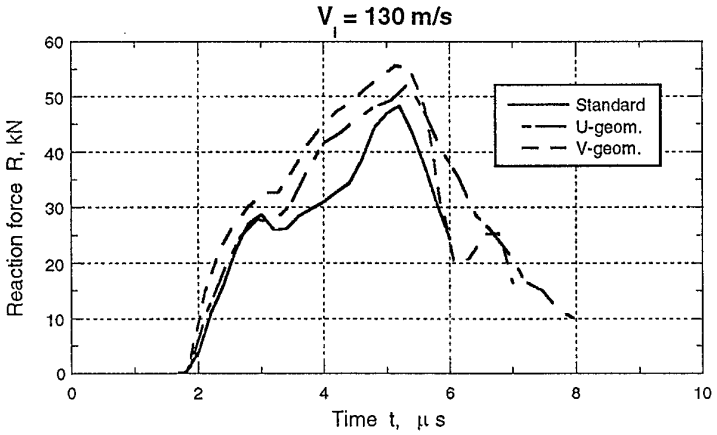
V_i = 130 m/s
Reaction force R, kN
Time t, μ s
Standard
U-geom.
V-geom.

c/

Fig. 14

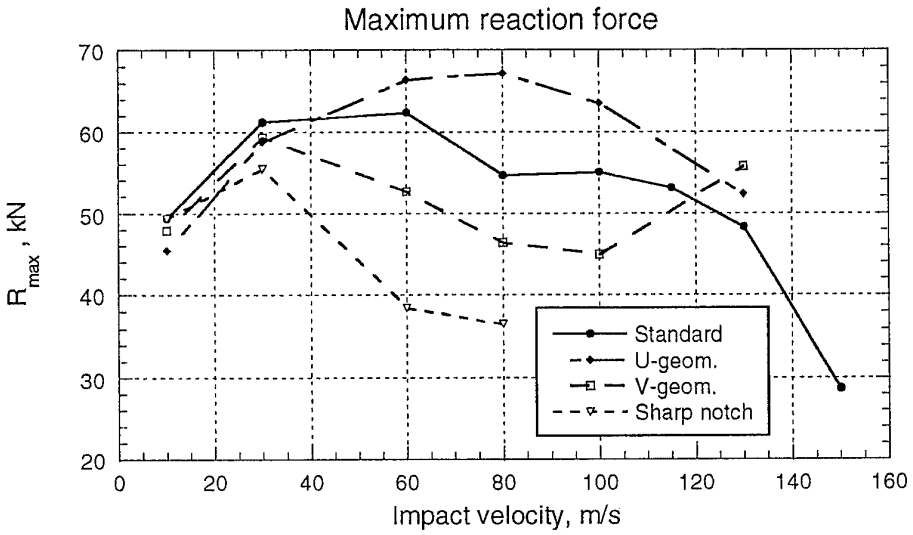
Maximum reaction force
70
60
50
40
30
20
R_{max}, kN
0
20
40
60
80
100
120
140
160
Impact velocity, m/s
Standard
U-geom.
V-geom.
Sharp notch

a/

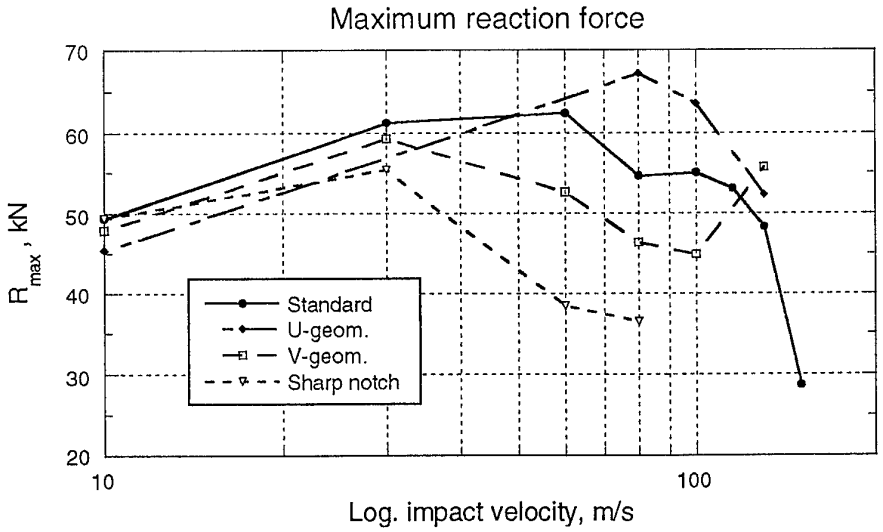
Maximum reaction force
70
60
50
40
30
20
R_{max}, kN
10
100
Log. impact velocity, m/s
Standard
U-geom.
V-geom.
Sharp notch

b/

Fig. 15

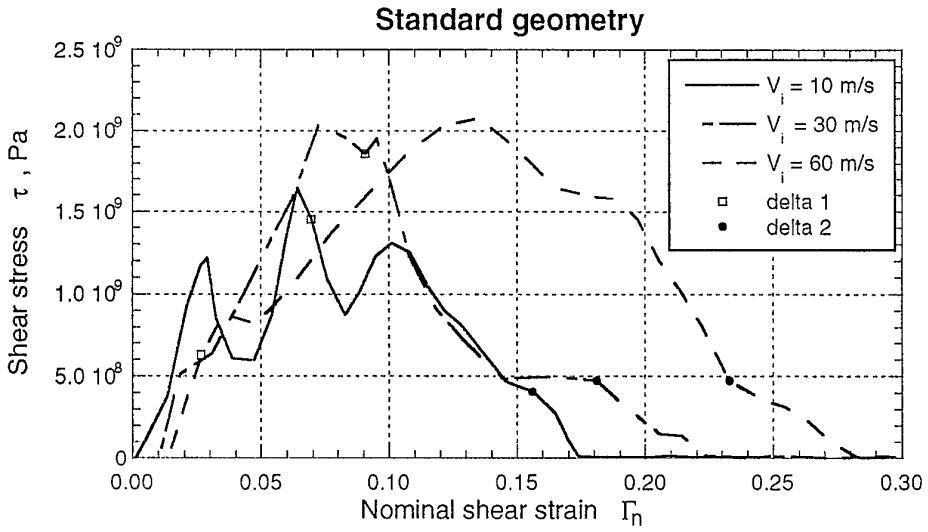
Standard geometry
Shear stress τ , Pa
2.5 10^9
2.0 10^9
1.5 10^9
1.0 10^9
5.0 10^8
0
0.00
0.05
0.10
0.15
0.20
0.25
0.30
Nominal shear strain Γn
V_i = 10 m/s
V_i = 30 m/s
V_i = 60 m/s
delta 1
delta 2

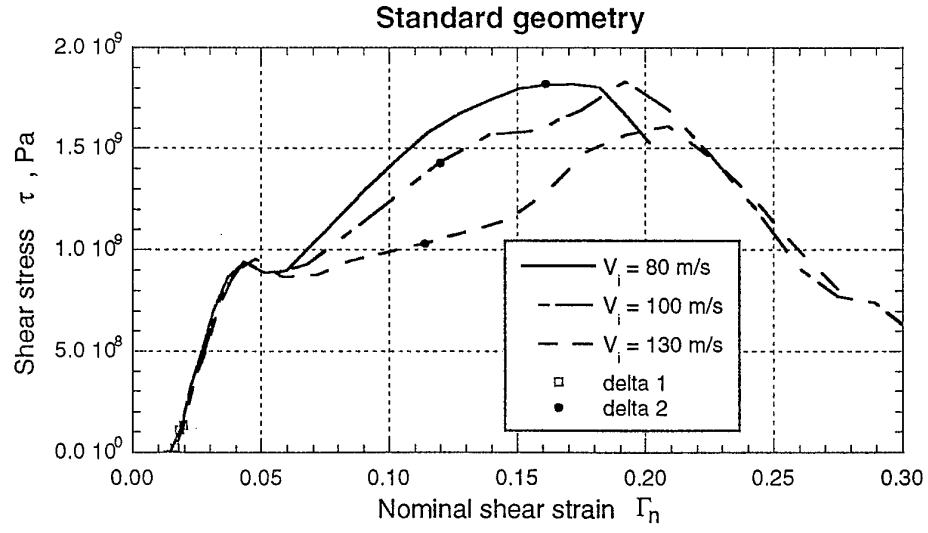
Standard geometry
Shear stress τ , Pa
2.0 10^9
1.5 10^9
1.0 10^9
5.0 10^8
0.0 10^0
0.00
0.05
0.10
0.15
0.20
0.25
0.30
Nominal shear strain Γn
V_i = 80 m/s
V_i = 100 m/s
V_i = 130 m/s
delta 1
delta 2

Fig. 16

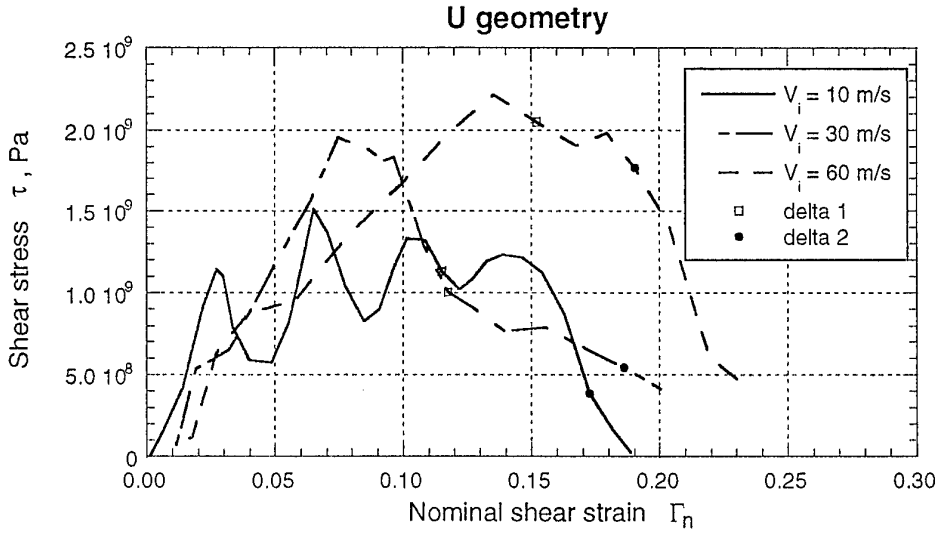
U geometry
Shear stress τ , Pa
2.5 10^9
2.0 10^9
1.5 10^9
1.0 10^9
5.0 10^8
0
0.00
0.05
0.10
0.15
0.20
0.25
0.30
Nominal shear strain Γn
V_i = 10 m/s
V_i = 30 m/s
V_i = 60 m/s
delta 1
delta 2

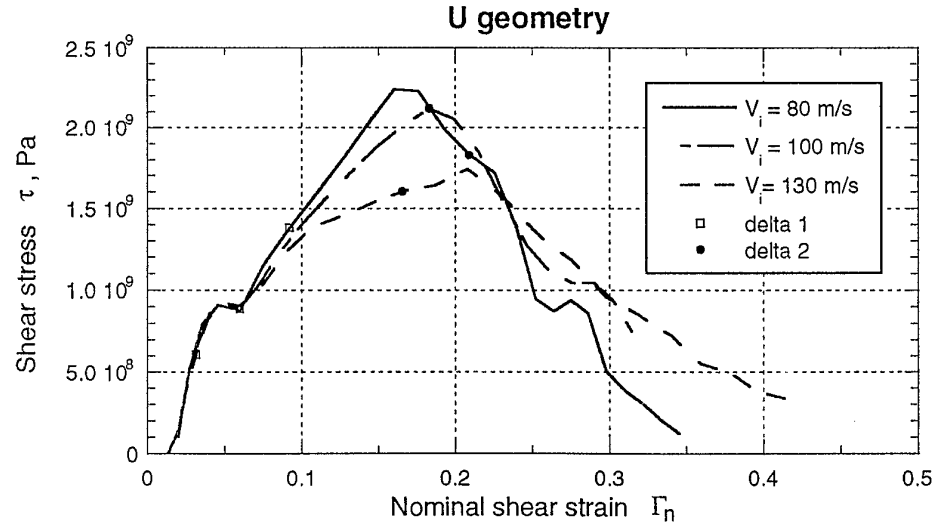
U geometry
Shear stress τ , Pa
2.5 10^9
2.0 10^9
1.5 10^9
1.0 10^9
5.0 10^8
0
0
0.1
0.2
0.3
0.4
0.5
Nominal shear strain Γn
V_i = 80 m/s
V_i = 100 m/s
V_i = 130 m/s
delta 1
delta 2

Fig. 17

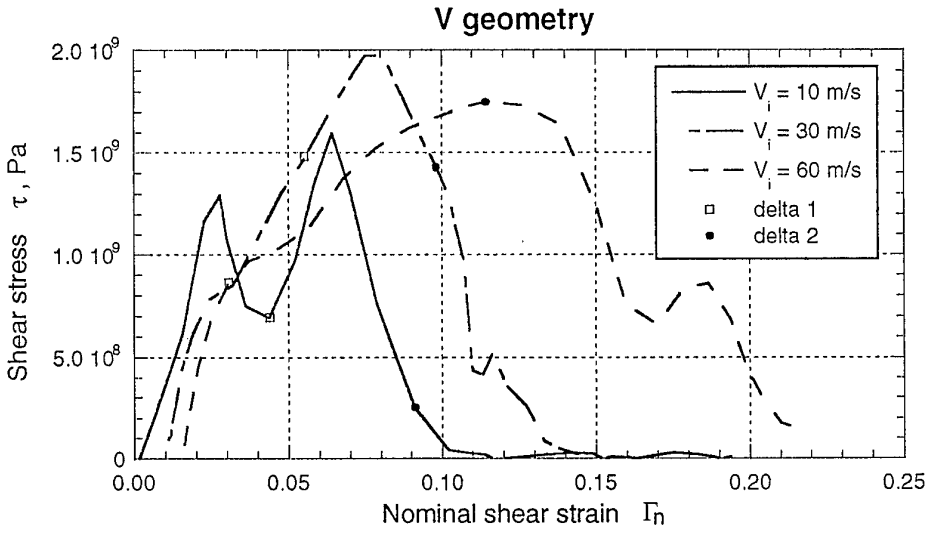
V geometry
2.0 10^9
1.5 10^9
1.0 10^9
5.0 10^8
0
Shear stress τ, Pa
0.00
0.05
0.10
0.15
0.20
0.25
Nominal shear strain Γn
V_i = 10 m/s
V_i = 30 m/s
V_i = 60 m/s
delta 1
delta 2

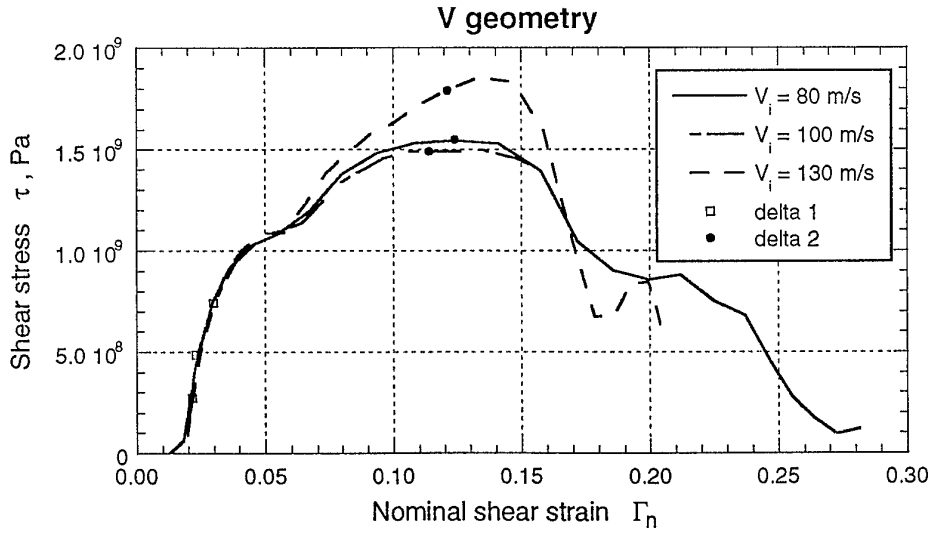
V geometry
2.0 10^9
1.5 10^9
1.0 10^9
5.0 10^8
0
Shear stress τ, Pa
0.00
0.05
0.10
0.15
0.20
0.25
0.30
Nominal shear strain Γn
V_i = 80 m/s
V_i = 100 m/s
V_i = 130 m/s
delta 1
delta 2

Fig. 18

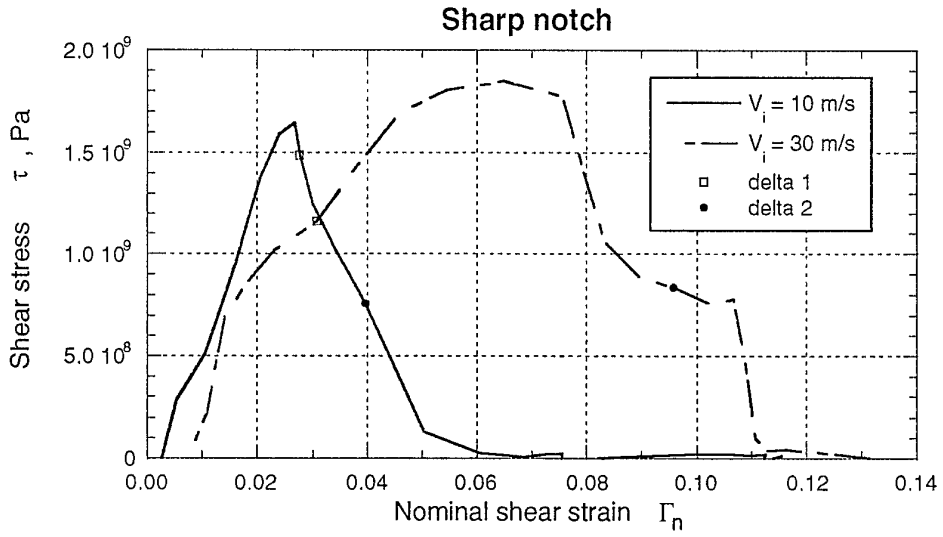
Sharp notch
Shear stress τ , Pa
2.0 10^9
1.5 10^9
1.0 10^9
5.0 10^8
0
0.00
0.02
0.04
0.06
0.08
0.10
0.12
0.14
Nominal shear strain Γn
V_i = 10 m/s
V_i = 30 m/s
delta 1
delta 2

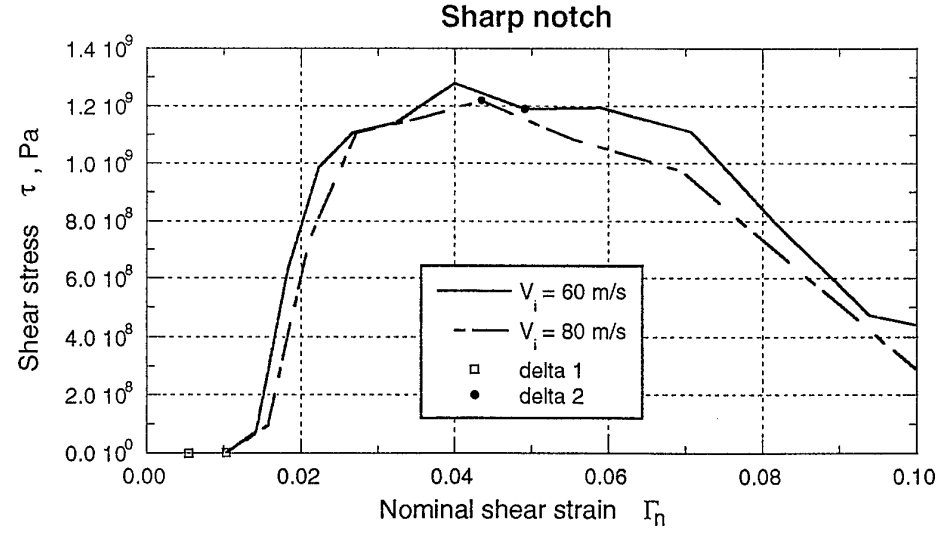
Sharp notch
Shear stress τ , Pa
1.4 10^9
1.2 10^9
1.0 10^9
8.0 10^8
6.0 10^8
4.0 10^8
2.0 10^8
0.0 10^0
0.00
0.02
0.04
0.06
0.08
0.10
Nominal shear strain Γn
V_i = 60 m/s
V_i = 80 m/s
delta 1
delta 2

Fig. 19